

NONLINEAR OPTICAL PHENOMENA https://doi.org/10.1070/QEL17211

$BaGa_2GeS_6$ and $BaGa_2GeSe_6$ crystals for nonlinear optical frequency conversion

S.G. Grechin, P.P. Nikolaev, A.A. Ionin, I.O. Kinyaevskii, Yu.M. Andreev

Abstract. **We analyse the functional capabilities of new crystals, $BaGa_2GeS_6$ (BGGS) and $BaGa_2GeSe_6$ (BGGSe), which are used for nonlinear optical frequency conversion in their transparency range. The wavelengths at which maximum conversion efficiencies can be obtained and the tuning range for difference-frequency generation are found. It is shown that there are wavelength combinations at which the effective nonlinearity coefficient varies only slightly in a wide frequency band.**

Keywords: *nonlinear crystals, $BaGa_2GeS_6$, $BaGa_2GeSe_6$, frequency conversion.*

One of the limitations hindering the development of high-power mid-IR lasers with frequency conversion is the low optical damage threshold of nonlinear crystals. For single nanosecond pulses in the wavelength range of 5–10 μm, the damage threshold for a majority of crystals is 50–200 MW cm^{-2} [1]. The loss factor also limits the average radiation power because of the thermal self-action in a crystal. In view of all these factors, synthesis of new nonlinear media is an urgent problem. Only since the beginning of this century more than 200 new crystals have been synthesised for operation in the mid-IR range. One of the last developments in this field is a series of barium halide crystals $BaGa_2MQ_6$ (M = Si, Ge; Q = S, Se) [2, 3]. $BaGa_2SiS_6$ (BGSS) and $BaGa_2SiSe_6$ (BGSSe) turned out to be chemically unstable, and all works were focused on the growth and investigation of sulfide $BaGa_2GeS_6$ (BGGS) and selenide $BaGa_2GeSe_6$ (BGGSe).

To date, all linear and nonlinear parameters of these crystals have not been measured with a sufficiently high accuracy. However, even the existing data make it possible to estimate the functional possibilities of BGGS and BGGSe crystals, which are used to solve all problems of nonlinear optical frequency conversion: generation of sum and difference frequencies and parametric generation. These issues are considered in this paper.

S.G. Grechin Prokhorov General Physics Institute, Russian Academy of Sciences, ul. Vavilova 38, 119991 Moscow, Russia;
e-mail: S.G.Grechin@mail.ru;
P.P. Nikolaev LLC Neofotonika, prosp. Obukhovskoi oborony 21A, 192019 St. Petersburg, Russia;
A.A. Ionin, I.O. Kinyaevskii Lebedev Physical Institute, Russian Academy of Sciences, Leninsky prosp. 53, 119991 Moscow, Russia;
Yu.M. Andreev Institute of Monitoring of Climatic and Ecological Systems, Siberian Branch, Russian Academy of Sciences, prosp. Akademicheskii 10/3, 634055 Tomsk, Russia

Received 29 November 2019
Kvantovaya Elektronika **50** (8) 782–787 (2020)
Translated by Yu.P. Sin'kov

Even the first studies showed good prospects of BGGS and BGGSe crystals. They are characterised by a wide range of transparency (from visible to mid-IR region) and large nonlinear susceptibility tensor coefficients d_{ij}. Since the band gap of BGGS and BGGSe crystals exceeds that of $AgGaS_2$ (AGS) and $AgGaSe_2$ (AGSe), one would expect BGGS and BGGSe to have a higher destruction threshold.

The issues concerning the synthesis of crystals and analysis of their parameters were considered in [2–6]. According to the data of [2], the BGGS crystal is transparent in the range of 0.380–13.7 μm. In [4], the transparency ranges were found to be 0.41–11.8 μm for BGGS and 0.58–12 μm for BGGSe. However, those publications lacked data on the anisotropy of absorption coefficients, which follow from the dispersion relations for transmittances [4].

The results of measuring the damage thresholds of BGGS and BGGSe crystals were reported in [7]. A single-shot Nd:YLF laser was used, which generated (5–17)-ns pulses at a wavelength of 1.053 μm. The measurements showed that the surface damage thresholds for both crystals are close and amount to 200–300 MW cm^{-2} at a pulse repetition rate of 0.1–1.0 kHz. With an increase in the rate from 100 Hz to 1 kHz, the damage threshold decreases by 10%–20% on average.

The Sellmeier coefficients for two positive crystals were measured for the first time in [4]. The expressions for these coefficients have the form

$$n_o = 5.1047 + \frac{0.1480}{\lambda^2 - 0.0562} - 0.00253\lambda^2, \quad (1)$$

$$n_e = 5.3488 + \frac{0.1674}{\lambda^2 - 0.0536} - 0.00265\lambda^2 \quad (2)$$

for the BGGSe crystal and

$$n_o = 6.1746 + \frac{0.2679}{\lambda^2 - 0.1174} - 0.00116\lambda^2, \quad (3)$$

$$n_e = 6.6022 + \frac{0.3030}{\lambda^2 - 0.1324} - 0.00121\lambda^2 \quad (4)$$

for the BGGSe crystal. Hereinafter, n_o and n_e are the principal values of refractive indices and λ is the radiation wavelength (in μm). More exact expressions for the BGGSe crystal in the range of 0.78–10.591 μm were obtained in [5] within the double-resonance model:

$$n_o = 7.39367 + \frac{0.27086}{\lambda^2 - 0.06961} + \frac{1513.10}{\lambda^2 - 1237.35}, \quad (5)$$

$$n_e = 8.11658 + \frac{0.30287}{\lambda^2 - 0.13199} + \frac{2197.51}{\lambda^2 - 1408.89}. \quad (6)$$

Below we use expressions (5) and (6) to calculate the phase-matching angles for the BGGSe crystal.

Both BGGS and BGGSe belong to the trigonal system with the point symmetry group 3. The nonlinear susceptibility tensor with two-index designation of elements has the form

$$d_{ij} = \begin{vmatrix} d_{11} & d_{12} & 0 & 0 & d_{15} & d_{16} \\ d_{21} & d_{22} & 0 & d_{24} & 0 & d_{26} \\ d_{31} & d_{32} & d_{33} & 0 & 0 & 0 \end{vmatrix}. \quad (7)$$

The expressions for the effective nonlinearity coefficients of positive crystals of this point group (under Kleinman symmetry conditions) can be presented in the form

$$d_{\text{eff}} = \cos^2\theta(d_{11}\sin 3\varphi + d_{22}\cos 3\varphi) \quad (8)$$

for the eeo-type interaction and

$$d_{\text{eff}} = \cos\theta(d_{11}\cos 3\varphi - d_{22}\sin 3\varphi) + d_{15}\sin\theta \quad (9)$$

for the eoo = oeo-type interaction. Here, φ is the azimuthal angle counted from the x axis in the xy plane, and θ is the polar angle (between the z axis and phase-matching direction).

Currently, there are no reliable experimental data on the nonlinear susceptibility tensor coefficients. The first measurements of these coefficients were based on comparing the second-harmonic intensities obtained using BGGS and BGGSe crystals and those obtained with AGS and AGSe crystals. The measurement results were reported in [2]. The measurements were performed by the powder method for particles 80–100 μm in size. The second-harmonic intensities obtained in sulfides BGGS and AGS and selenides BGGSe and AGSe with a laser having a wavelength $\lambda = 2.09$ μm turned out to be close.

Similar measurements were performed in [3] using the rule proposed in [8]. The measurements showed that the nonlinearity coefficient for the second-harmonic generation (SHG) of radiation with $\lambda = 2.05$ μm in BGGS and BGGSe crystals is higher than that in AGS crystals by factors of ~2.1 and ~3.5, respectively. Based on these data, the authors found the effective nonlinearity coefficients to be 26.3 pm V^{-1} for BGGS and 43.7 pm V^{-1} for BGGSe.

An attempt was made in [4] to determine the tensor coefficients d_{ij} from the results of measuring the SHG efficiency for CO_2 laser radiation ($\lambda = 10.6$ μm) in a homogeneous BGGSe crystal. A value $d_{11} = 66 \pm 15$ pm V^{-1} was obtained. Using this result, the effective nonlinearity coefficient for the first-type interaction was found to be $d_{\text{eff}} = 47.5$ pm V^{-1} in [4], and a value $d_{\text{eff}} = 14.4$ pm V^{-1} was reported for the second-type interaction. However, since the measurement and data processing technique used in [4] contain errors, the aforementioned values are overestimated. The data processing technique used in [4] was refined in [9], and the refined values were as follows: coefficient $d_{11} = 49 \pm 15$ pm V^{-1} and effective nonlinearity coefficient of SHG for a CO_2 laser $d_{\text{eff}} = 42 \pm 14$ pm V^{-1}. Nevertheless, the data obtained are insufficient to calculate d_{eff} for an arbitrary wavelength.

The results of calculating the nonlinear susceptibility tensor coefficients d_{ij} for $BaGa_2MQ_6$ crystals (M = Si, Ge; Q = S, Se) using the plane-wave pseudopotential method [8] were reported in [2]. The calculation results [2] for BGGS and BGGSe crystals are listed in Table 1. Using these data, one cannot obtain the effective nonlinearity coefficients reported in [3]. However, at this stage we will use the data of Table 1 to calculate d_{eff}. The refinement of d_{ij} values will change quantitatively the results presented below, but, on the whole, should not change them qualitatively.

Table 1. Tensor coefficients d_{ij}.

Crystal	d_{ij}/pm V^{-1}			
	d_{11}	d_{15}	d_{22}	d_{33}
BGGS	5.6	9.4	10.5	–12.0
BGGSe	13.0	24.7	–27.4	–23.0

Distributions of effective nonlinearity coefficients of BGGS and BGGSe crystals for two interaction types are shown in Fig. 1. Note that data on only one crystal of point group 3 ($Nd:LaBGeO_5$) were reported in [1]. A characteristic feature of the distributions in Fig. 1 for the eeo-type interaction is as follows. Despite the fact that the argument of harmonic functions in (8) is 3φ, the values of azimuthal angle $\varphi_{\max}$ at which d_{eff} is maximum are not equal to $m\times 30°$ ($m = 0, 1, 2, \ldots$) because of the difference in the moduli of coefficients d_{11} and d_{22}. The angle $\varphi_{\max}$ can easily be found from the condition $\mathrm{d}d_{\text{eff}}/\mathrm{d}\varphi = 0$. As a result, we arrive at

$$\varphi_{\max} = \frac{1}{3}\arctan\left(\frac{d_{11}}{d_{22}}\right).$$

This feature also manifests itself in the distributions for the (eoo = oeo)-type interaction (Figs 1b, 1d).

It follows from Fig. 1 that angular-noncritical phase matching cannot be implemented for the eeo-type interaction. It may occur for the (eoo = oeo)-type interaction, but at a

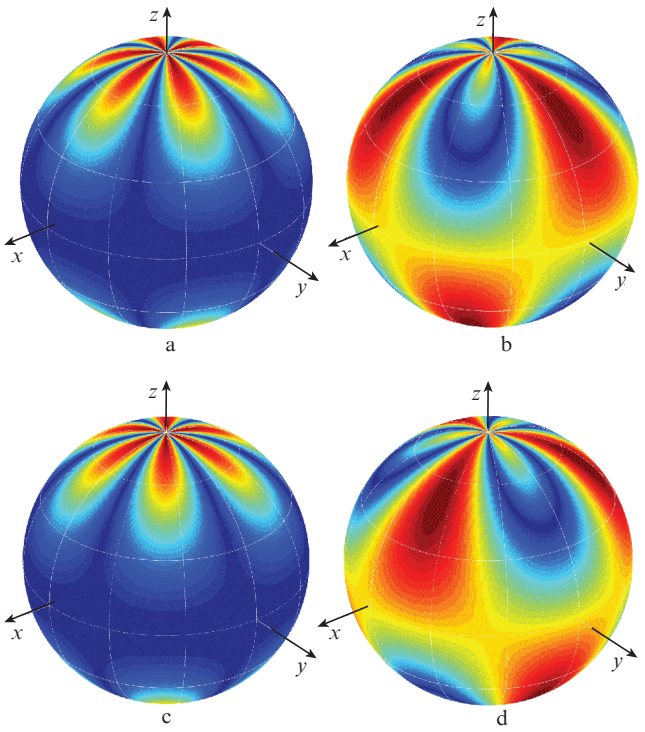

Figure 1. (Colour online) Distributions of effective nonlinearity coefficients of (a, b) BGGS and (c, d) BGGSe crystals for the (a, c) eeo- and (b, d) (eoo = oeo)-type interactions.

much smaller effective nonlinearity coefficient, which can be obtained for the optimal angle θ.

The determination of the functional possibilities of crystals used to solve all frequency-conversion problems is based on the method for analysing uniaxial and biaxial crystals, which was proposed in [10, 11]. This method involves representation of the parameter $FOM_2 = d_{eff}^2/(n_1n_2n_3)$ as a dependence on the wavelengths λ_1 and λ_2 – $FOM_2(\lambda_1, \lambda_2)$. Here, n_i are the refractive indices for the interacting waves: $n_1(\lambda_1)$, $n_2(\lambda_2)$, $n_3(\lambda_3)$; $\lambda_1 \geqslant \lambda_2 \geqslant \lambda_3$. This parameter is determined by the maximum value d_{eff} on the phase-matching curve with a change in the angles φ and θ. Specifically this crystal cut is chosen in practice to obtain a maximum conversion efficiency. This method turned out to be adequate when studying the properties of KTP crystal and its isomorphs [12], as well as the PIT crystal [13].

The dependences $FOM(\lambda_1, \lambda_2)$ for interactions of all types in BGGS and BGGSe crystals are presented in Fig. 2. The solid lines correspond to $\lambda_3 = (1/\lambda_1 + 1/\lambda_2)^{-1}$. The vertical and horizontal dot-dashed lines show the applicability limits for the Sellmeier equation, which were determined in [5]. A detailed description of the results that can be obtained from the reported distributions $FOM_2(\lambda_1, \lambda_2)$ can be found in [10, 11].

It can be seen in Fig. 2 that the effective nonlinearity coefficient is maximum for the BGGSe crystal. For the oeo- and eoo-type interactions, the $FOM_2(\lambda_1, \lambda_2)$ value may reach 100 $pm^2\ V^{-2}$. For the eeo-type interaction, this value is almost two times smaller. For the BGGS crystal, all the $FOM_2(\lambda_1, \lambda_2)$ values are five to six times smaller than for BGGSe. The lower boundary of all $FOM_2(\lambda_1, \lambda_2)$ distributions corresponds to the angular-noncritical phase matching ($\theta = 90°$). As was noted above, $d_{eff} = 0$ in both crystals for the eeo-type interaction at this value of the angle, which implies that the phase matching is present but the medium nonlinearity is equal to zero.

Various frequency conversion processes may occur in the crystals under consideration in a wider part of transparency range. The character of distributions of d_{eff} in Fig. 1 shows that the wavelength range in which the conversion efficiency is maximum is wider for the oeo- and eoo-type interactions than for the eeo-type interaction. The phase-matching conditions are known to be satisfied initially for the first-type interaction within the crystal transparency range. This range determines the minimum and maximum fundamental laser wavelengths that allow for second-harmonic generation. It follows from Fig. 2 for the eeo-type interaction that the minimum fundamental wavelengths at SHG for the BGGS and BGGSe crystals are, respectively, 1.7 and 1.8 μm. SHG in BGGS and BGGSe crystals can be implemented at wavelengths not larger than 12 μm.

Under SHG conditions in the case of oeo-type interaction, high conversion efficiency in BGGS and BGGSe crystals can be obtained in the ranges of 6–7 μm and 3–12 μm, respectively. The maximally efficient conversion in BGGSe occurs at wavelengths $\lambda_1 = \lambda_2$ in the range of 8–11 μm. The maximally efficient third-harmonic generation (THG) in the BGGS and BGGSe crystals is implemented in the ranges of 6–8 μm and 4–12 μm, respectively.

For the eoo-type interaction, high conversion efficiency for SHG in the BGGS and BGGSe crystals can be obtained in the ranges of 3–6 μm and 3–12 μm, respectively. THG is impossible in the BGGS crystal, whereas in the BGGSe crystal it may occur in the range of 4–12 μm.

Using radiation at $\lambda_3 = 1.0$ μm, one can implement difference-frequency generation (DFG) in the crystals under consideration. In this case, radiation in a wide wavelength range (from 3.0 to 12 μm) can be obtained for both eoo- and oeo-type interactions. For the eeo- and oeo-type interactions, the phase-matching properties of crystals provide radiation under pumping at a wavelength of 1.0 μm. However, the d_{eff} value is very small in the range of $\lambda_1 = 2$–7 μm. The tuning range in both crystals may vary from 6–7 to 12 μm. Therefore, the total tuning range is fairly wide, whereas the working range is limited. The tuning ranges for all interaction types and wavelengths $\lambda_3 = 1.0$, 1.5, and 2.0 μm are listed in Table 2.

Table 2. Tuning ranges for radiation wavelength λ_1 in the DFG regime.

Crystal	Type	λ_3/μm	Range	λ_1/μm
BGGS	eeo	1.0	total	2–12
	eeo	1.0	working	6–12
	eeo	1.5	working	3–12
	eeo	2.0	working	4–12
	oeo	1.0	working	2.5–12
	oeo	1.5	working	3–12
	oeo	2.0	working	4.2–12
	eoo	1.0	–	–
	eoo	1.5	working	3–5
	eoo	2.0	working	4–7
BGGSe	eeo	1.0	total	2–12
	eeo	1.0	working	7–12
	eeo	1.5	working	3–12
	eeo	2.0	working	4–12
	oeo	1.0	working	2.5–12
	oeo	1.5	working	3–12
	oeo	2.0	working	4.2–12
	eoo	1.0	–	–
	eoo	1.5	working	3–12
	eoo	2.0	working	4.3–12

For the oeo- and eoe-type interactions, there are wide spectral ranges in BGGS and BGGSe crystals, where the $FOM_2(\lambda_1, \lambda_2)$ values barely change. This feature differs significantly these crystals from the uniaxial crystals of other point groups [10]. The distributions $FOM_2(\lambda_1, \lambda_2)$ in Fig. 2 are in fact distributions of d_{eff} values. It follows from expressions (8) and (9) that there is a direct relationship between the phase-matching angle and coefficient d_{eff}. Thus, we find that the phase-matching angle does not change in a fairly wide range of $FOM_2(\lambda_1, \lambda_2)$ distributions. This situation corresponds to the frequency-noncritical phase matching (FNCPM) regime.

Figure 3 shows the $FOM_2(\lambda_1, \lambda_2)$ distribution for the oeo-type interaction in BGGSe crystal. The straight lines in this figure are the directions corresponding to specified relations between the wavelengths λ_1 and λ_2: $\lambda_1 = \lambda_2$ (SHG), $\lambda_2 = 0.75\lambda_1$ [sum-frequency generation (SFG)], and $\lambda_2 = 0.5\lambda_1$ (THG). Figure 4 shows the dependences of phase-matching angle and $FOM_2(\lambda_1, \lambda_2)$ on λ_1 for these three cases.

The dependences of phase-matching angles on λ_1 (Fig. 4a) are on the whole similar to those observed for uniaxial crystals [10]. The minimum θ_{phm} values for the BGGSe crystal were obtained at λ_1 = (*1*) 5.5, (*2*) 6.5, and (*3*) 7.8 μm. They correspond to the FNCPM regime. However, the dependence of $FOM_2(\lambda_1, \lambda_2)$ on λ_1 (Fig. 4b) differs qualitatively from the dependences presented in Fig. 4a. They barely change in a wide wavelength range. This is related to the character of

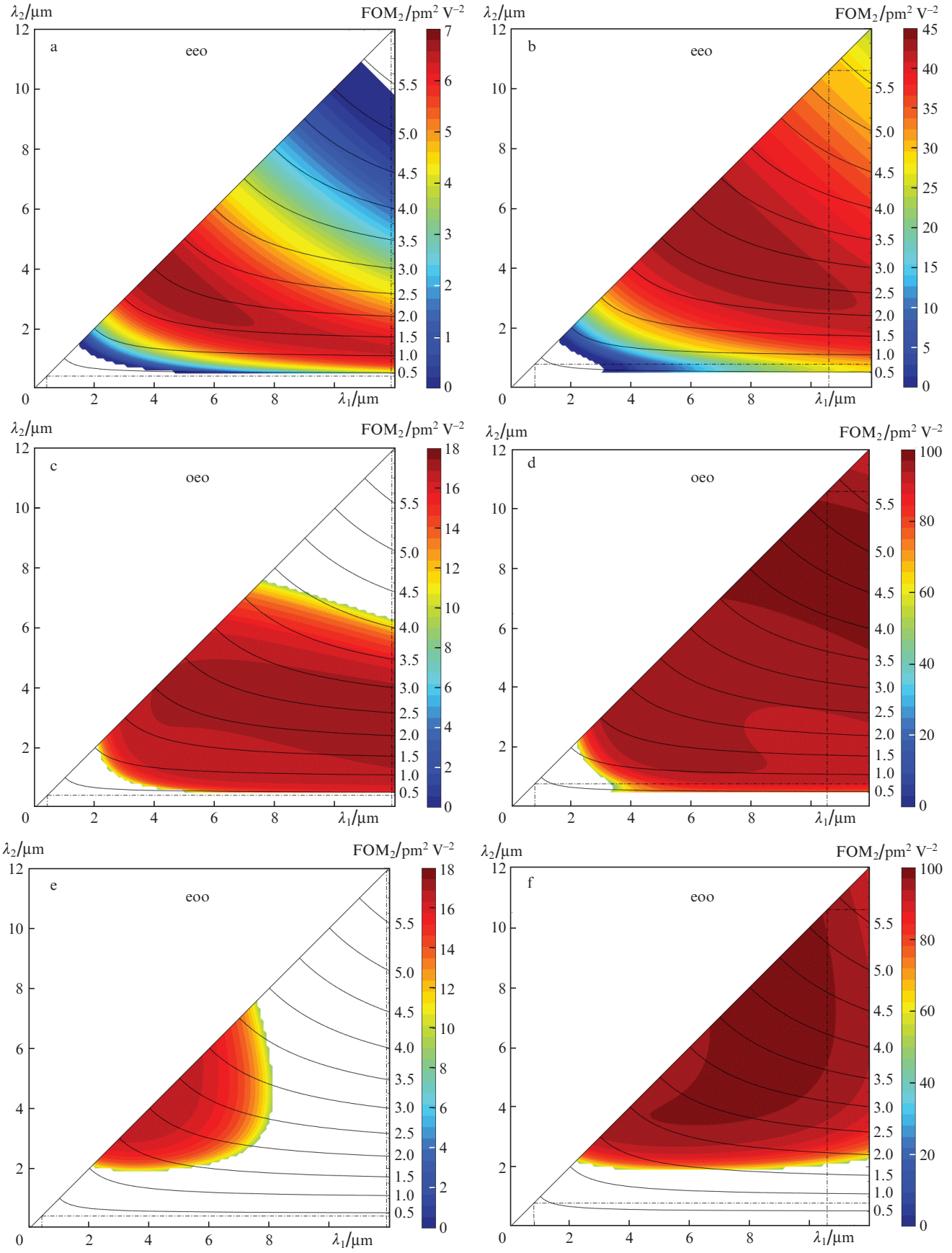

Figure 2. (Colour online) Distributions $FOM_2(\lambda_1, \lambda_2)$ for (a, c, e) BGGS and (b, d, f) BGGSe crystals and interactions of (a, b) eeo, (c, d) oeo, and (e, f) eoo types.

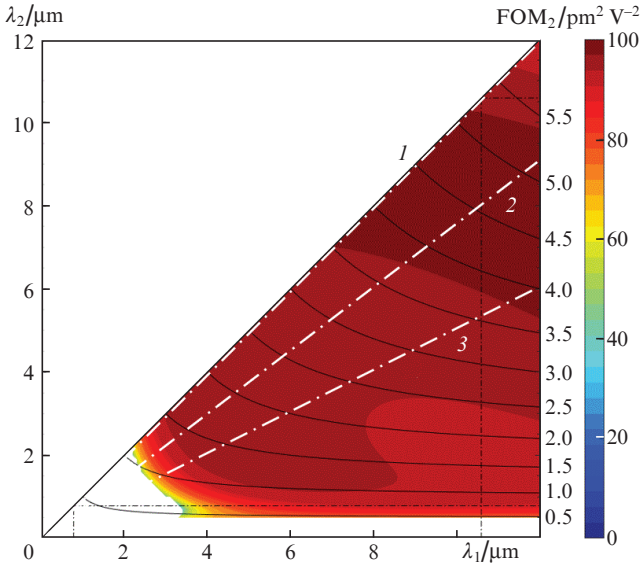

Figure 3. Distribution $FOM_2(\lambda_1, \lambda_2)$ for the oeo-type interaction in BGGSe crystal at $\lambda_1 = (1)\,\lambda_2$, $(2)\,0.75\lambda_1$, and $(3)\,0.5\lambda_1$

$FOM_2(\lambda_1, \lambda_2)$ distribution in dependence of the angles φ and θ (Fig. 1b). The $FOM_2(\lambda_1, \lambda_2)$ value (Fig. 4b) changes very slowly in a fairly wide range of variation in the angle θ_{phm} (Fig. 4a). In particular, a decrease in the maximum $FOM_2(\lambda_1, \lambda_2)$ value by 5% in Fig. 4b occurs in the ranges of (*1*) 3.0–12, (*2*) 3.75–12, and (*3*) 5.3–12 μm. The FNCPM regime was implemented in these ranges. The coincidence of the regions of slow variation in $FOM_2(\lambda_1, \lambda_2)$ and phase-matching angle under the FNCPM conditions leads to the formation of a distribution of similar shape with a large spectral width.

In the case of frequency conversion for pulsed femtosecond radiation, high radiation intensities make it possible to use crystals with a length of no more than 1 mm. In this situation, the angular phase-matching width for a majority of crystals is no less than 20° even under conditions of angular-critical phase matching. Generally the dependence of $FOM_2(\lambda_1, \lambda_2)$ on, e.g., λ_1, has a shape similar to that of the dependence of phase-matching angle on λ_1. A pronounced extremum and a fairly rapid decrease in $FOM_2(\lambda_1, \lambda_2)$ are observed in the case of frequency mismatch. The results for the BGGSe crystal (Fig. 4b) show that there are conditions for equiefficient conversion of all frequency components. This is valid for different nonlinear optical frequency converters with wavelength tuning and for optical parametric oscillators. A detailed analysis of the prospects of implementing the FNCPM regime at different wavelengths will be performed after obtaining more exact data on the crystal parameters.

The distributions in Fig. 2 correspond to homogeneous BGGS and BGGSe crystals. Their difference shows that the distributions may change significantly for mixed $BaGa_2S_xSe_{6-x}$ crystals.

We reported the preliminary results of analysing the functional possibilities of new nonlinear crystals, BGGS and BGGSe. It was shown that frequency conversion can be implemented in the visible to mid-IR range. The possible wavelength tuning range in the DFG regime was determined. It was found that a weakly changing effective nonlinearity coefficient can be obtained at some wavelength combinations. This circumstance makes it possible to perform effective frequency conversion of radiation, both with a wide wavelength tuning range and with a large spectral width.

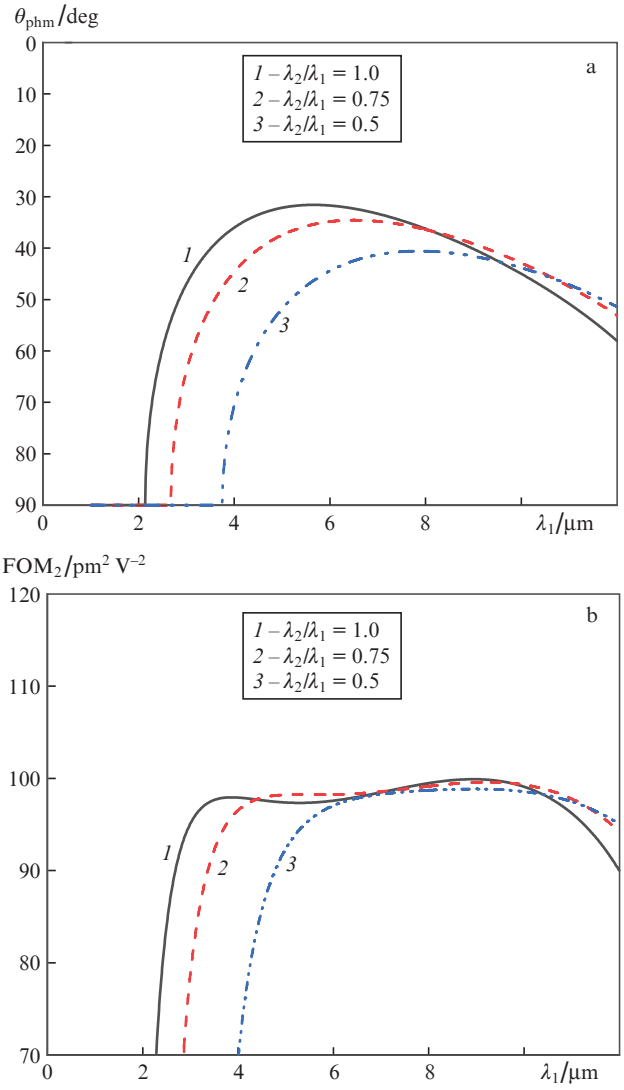

Figure 4. Dependences of the (a) phase-matching angle and (b) $FOM_2(\lambda_1, \lambda_2)$ on λ_1 for the BGGSe crystal at $\lambda_1 = (1)\,\lambda_2$ (SHG), $(2)\,0.75\lambda_1$ (SFG), and $(3)\,0.5\lambda_1$ (THG).

Despite the absence of exact data on the parameters of nonlinear crystals under study, our analysis showed their good prospects for designing optical parametric oscillators pumped by near-IR lasers and for generating the second and third harmonics of mid-IR laser radiation.

Acknowledgements. This work was performed within State Budget Programme No. AAAA-A17-117013050036-3.

References

1. Nikogosyan D.N. *Nonlinear Optical Crystals: A Complete Survey* (New York: Springer, 2005).
2. Lin X., Guo Y., Ye N., Zhai N. *J. Solid State Chem.*, **195**, 172 (2012).
3. Yin W., Feng K., He R., Mei D., Lin Z., Yao J., Wu Y. *Dalton Trans.*, **41**, 5653 (2012).
4. Badikov V.V., Badikov D.V., Laptev V.B., Mitin K.V., Shevyrdyaeva G.S., Shchebetova N.I., Petrov V. *Opt. Mater. Express*, **6**, 2933 (2016).

5. Kato K., Miyata K., Badikov V.V., Petrov V. *Appl. Opt*., **57**, 7440 (2018).
6. Kurtz S.K., Perry T.T. *Appl. Phys*., **39**, 3798 (1968).
7. Kostyukova N.Y., Boyko A.A., Erushin E.Y., Kostyukov A.I., Badikov V.V., Badikov D.V., Kolker D.B. *J. Opt. Soc. Am. B*, **36**, 2260 (2019).
8. Payne M.C., Teter M.P., Allan D.C., Arias T.A., Joannopoulos J.D. *Rev. Mod. Phys*., **64**, 1045 (1992).
9. Badikov D.V., Badikov V.V., Ionin A.A., Kinyaevskiy I.O., Klimachev Yu.M., Kotkov A.A., Mitin K.V., Mokrousova D.V., Mojaeva V.A. *Opt. Quantum Electron*., **50**, 243 (2018).
10. Andreev Yu.M., Arapov Yu.D., Grechin S.G., Kos'yanov I.V., Nikolaev P.P. *Quantum Electron*., **46**, 33 (2016) [*Kvantovaya Elektron*., **46**, 33 (2016)].
11. Andreev Yu.M., Arapov Yu.D., Grechin S.G., Kos'yanov I.V., Nikolaev P.P. *Quantum Electron*., **46**, 995 (2016) [*Kvantovaya Elektron*., **46**, 995 (2016)].
12. Gagarskiy S., Grechin S., Druzhinin P., Kato K., Kochiev D., Nikolaev P., Umemura N. *Crystals*, **8**, 386 (2018).
13. Grechin S.G., Nikolaev P.P., Andreev Yu.M. *Laser Phys*., **29**, 105101 (2019).